SPECTRAL OBSERVATIONS OF ENVELOPES AROUND STARS IN LATE STAGES OF STELLAR EVOLUTION

T. Blöcker[1], K.-H. Hofmann[1] and G. Weigelt[1]

Abstract. Interferometric observations of stars in late stages of stellar evolution and the impact of VLTI observations are discussed. Special attention is paid to the spectral information that can be derived from these observations and on the corresponding astrophysical interpretation of the data by radiative transfer modelling. It is emphasized that for the robust and non-ambiguous construction of dust-shell models it is essential to take diverse and independent observational constraints into account. Apart from matching the spectral energy distribution, the use of spatially resolved information plays a crucial role for obtaining reliable models. The combination of long-baseline interferometry data with high-resolution single-dish data (short baselines), as obtained, for example, by bispectrum speckle interferometry, provide complementary information and will improve modelling and interpretation.

1 Introduction: Late stages of stellar evolution

The Very Large Telescope Interferometer (VLTI; see Glindemann, this volume) of the European Southern Observatory with its four 8.2 m unit telescopes (UTs) and three 1.8 m auxiliary telescopes (ATs) will certainly establish a new era of studying the late stages of stellar evolution within the next few years. With a maximum baseline of up to more than 200 m, the VLTI will allow observations with unprecedented resolution opening up new vistas to a better understanding of the physics of evolved stars and thus of stellar evolution.

Stars in late stages of stellar evolution form therefore an important group among the VLTI key targets. During the Red Giant phase, strong winds erode the stellar surfaces leading to the formation of circumstellar shells which absorb an increasing fraction of the visible light and re-emit it in the infrared regime. Accordingly, most of these evolved stars are bright infrared objects. The heavy mass loss leads to the chemical enrichment of the interstellar medium and therefore plays a crucial role for the understanding of the galactic chemodynamical evolution.

---

[1] Max-Planck-Institut für Radioastronomie, Bonn, Germany

The vast majority of all stars, which have left their main sequence phase and become Red Giants, are of low and intermediate mass and finally evolve along the Asymptotic Giant Branch (AGB). These luminous, frequently pulsating and heavily mass-losing AGB stars form an important stellar population which contributes considerably to light, chemistry and dynamics of galaxies. The envelopes of AGB stars are the major factories of cosmic dust. Accordingly, AGB stars are often heavily enshrouded by dust exposing high fluxes in the infrared and are ideal laboratories to investigate the interplay between various physical and chemical processes. Most dust shells around AGB stars are known to be spherically symmetric on larger scales, whereas most objects in the immediate successive stage of proto-planetary nebulae appear in axisymmetric geometry. Evidence is growing that this break of symmetry takes place already at the very end of the AGB evolution.

Mass loss is also one of the dominant effects during the evolution of massive stars, virtually leading to an almost complete peeling of the star. Circumstellar dust shells found around evolved massive supergiants often show features of non-spherical outflows. Observing and modelling the circumstellar shells surrounding these stars, unveil details of evolution as, for instance, mass-loss rates. The presence of fossil shells even gives clues for the evolutionary history.

Dust formation around evolved stars can even continue beyond the Red Giant stage, as, e.g., in R CrB stars or late-type Wolf-Rayet stars. The production of dust in such hostile environments is still challenging to theory. In the instance of Wolf-Rayet stars colliding winds due to binarity is one of the favored scenarios.

High-resolution interferometric observations reveal details of disks and dust shells of evolved stars and thus improve our knowledge of, for example, the mass-loss process and its evolution. In the following sections, we discuss high spatial resolution observations and their interpretation by radiative transfer calculations for some prominent evolved stars.

2   Bispectrum speckle interferometry

The refractive index variations in the atmosphere of the earth restrict the angular resolution of large ground-based telescopes to $\sim 0''\!.5$ which is much worse than the theoretical diffraction limit ($\sim 0''\!.01$ for a 8 m telescope at optical wavelenghts). However, the atmospheric image degradation can be overcome and diffraction-limited images can be obtained either by adaptive optics (see, e.g., Tyson et al. 2002, Brandner et al. 2002) or bispectrum speckle interferometry (Weigelt 1977, Lohmann et al. 1983, Hofmann & Weigelt 1986). Speckle interferograms are images recorded with exposure times of ~ 50 ms in order to "freeze" the atmospheric turbulence. They consist of many small bright dots, called speckles, which are interference maxima of the incident light. The speckles are typically of the size of the theroretical Airy pattern of the aberration-free telescope. Fig. 1. shows a speckle interferogram of γ Ori (6 m telescope, $\lambda \sim 500$ nm) for illustration. Bispectrum speckle interferometry consists, in principle, of four steps: (i) calculation of the average bispectrum of all speckle interferograms; (ii) compensation of the
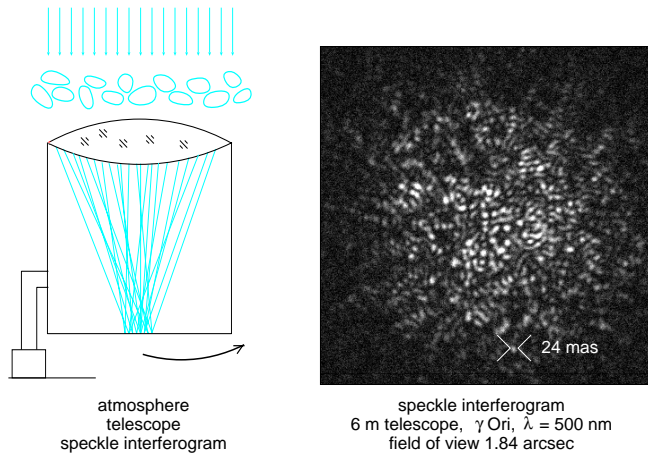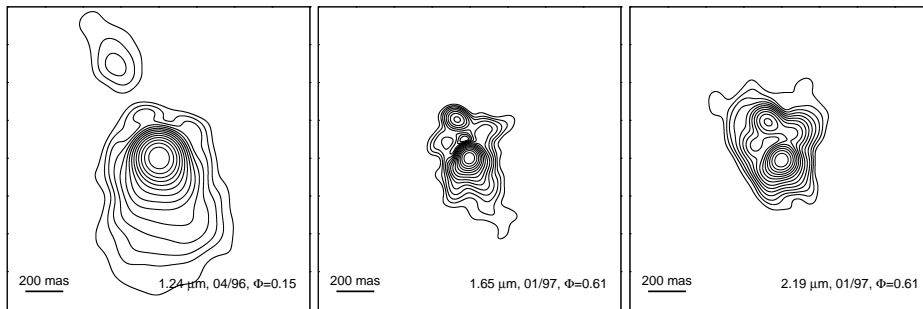
Fig. 1. Speckle interferogram of γ Ori.

atmosphere
telescope
speckle interferogram

speckle interferogram
6 m telescope, γ Ori, λ = 500 nm
field of view 1.84 arcsec

200 mas   1.24 µm, 04/96, Φ=0.15

200 mas   1.65 µm, 01/97, Φ=0.61

200 mas   2.19 µm, 01/97, Φ=0.61

Fig. 2. Speckle reconstructions of IRC +10 216 in J (left, Apr 1996, resolution 146 mas), H (middle, Jan 1997, resolution 73 mas), and K (right, Jan 1997, resolution 90 mas) Contour lines are shown from 0.3 mag to 4.2 mag relative to the peak brightness in steps of 0.3 mag. North is up and east is to the left (Osterbart et al. 2000).
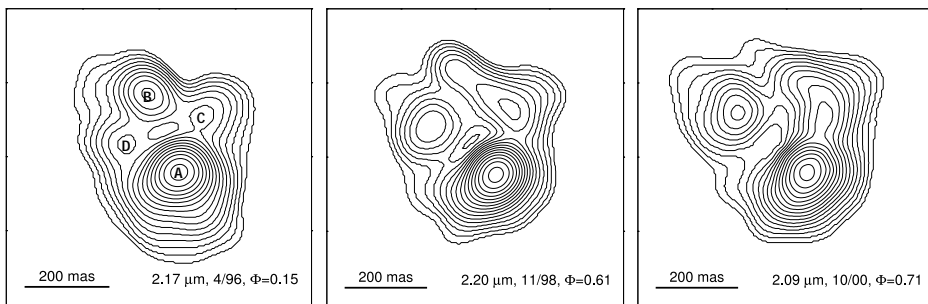

200 mas   2.17 µm, 4/96, Φ=0.15

200 mas   2.20 µm, 11/98, Φ=0.61

200 mas   2.09 µm, 10/00, Φ=0.71

Fig. 3. K-band speckle reconstructions of IRC +10 216 in 1996 (left), 1998 (middle), and 2000 (right). The resolution is 82 mas, 75 mas, and 73 mas, resp. Contour levels are plotted from 0.1 mag to 3.1 mag relative to the peak intensity in steps of 0.2 mag. North is up and east is to the left (Weigelt et al. 2002).

photon bias in the bispectrum; (iii) compensation of the speckle transfer function which can be derived from the speckle interferograms of a point source; and (iv) derivation of modulus and phase of the object Fourier transform from the bispectrum. In other words, bispectrum speckle interferometry with a single large telescope covers simultaneously all baselines up to the single telescopes's aperture size.

3 Interpreting the observations: Radiative transfer models

As discussed above, evolved stars are often surrounded by dust shells. An appropriate tool to interpret interferometric observations of dust shells are radiative transfer calculations. In order to handle the numerical effort to solve this complex problem, various assumptions have usually to be made with regard to the dust-shell geometry (spherical/2d/3d), dust formation (instantaneous/chemical network), and hydrodynamics (stationary/time-dependent). For example, the spherical radiative transfer problem can be solved by utilizing the self-similarity and scaling behaviour of IR emission from radiatively heated dust (Ivezić & Elitzur 1997). To tackle this problem including absorption, emission and scattering, several properties of the central source and its surrounding envelope are required, viz. (i) the spectral shape of the central source's radiation; (ii) the dust properties, i.e. the grains' optical constants and the grain size distribution, as well as the dust temperature at the inner boundary; (iii) the relative thickness of the envelope, i.e. the ratio of outer to inner shell radius, and the density distribution; and (iv) the total optical depth at a given reference wavelength. A two-dimensional approach of the radiative transfer problem is applied in, e.g., Men'shchikov et al. (2001), a hydrodynamic approach with explicit consideration of dust nucleation is given in Winters et al. (2000).

Radiative-transfer models have often to rely only on the comparison with the observed spectral energy distribution. However, high-resolution spatial information has proven to be an essential and complementary ingredient of dust-shell modelling. Only if such information is available, reliable, i.e. non-ambiguous, radiative-transfer models can be constructed and sound conclusions on the mass-loss process drawn (see e.g. Blöcker et al. 1999, 2001). In the following sections, we give three examples (IRC+10216, CIT 3, and IRC+10420) for such modelling.

4 The carbon star IRC+10216

The carbon star IRC +10 216 is a long-period AGB star suffering from a strong stellar wind (several 10^{-5} M$_\odot$/yr; Loup et al. 1993) which have led to an almost complete obscuration of the star by dust. Due to the high mass-loss rate, long period of $P = 649$ d (Le Bertre 1992), and carbon-rich chemistry of the dust-shell, IRC +10 216 is obviously in a very advanced stage of its AGB evolution. High-resolution near-infrared imaging of IRC +10 216 has revealed that on sub-arcsecond scales (100 mas) its dust shell is clumpy, bipolar, and changing on a time scale of

only ∼1 yr (Weigelt et al. 1997, 1998, Haniff & Buscher 1998, Osterbart et al. 2000, Tuthill et al. 2000, Weigelt et al. 2002). Since most dust shells around AGB stars are known to be spherically symmetric, whereas most proto-planetary nebulae (PPN) show an axisymmetric geometry (Olofsson 1996), it appears likely that IRC +10 216 has already entered the transition phase to the PPN stage. This suggests that the break of the dust-shell symmetry between the AGB and post-AGB phase already takes place at the end of the AGB evolution.

Bispectrum speckle-interferometry observations of IRC +10 216 were carried out with the SAO 6 m telescope in the J, H, and K band by Osterbart et al. (2000) and Weigelt et al. (2002) covering eight epochs between 1995 and 2001. Fig. 2 illustrates the different appearance of the dusty environment of IRC +10 216 in the J, H, and K bands. Fig. 3 shows the reconstructed K-band images of the innermost region of IRC +10 216 in 1996, 1998 and 2000. The dust shell consists of several compact components, at the beginning within a radius of 200 mas, which steadily change in shape and brightness. For instance, the apparent separation of the two initially brightest components A and B increased from 201 mas in 1996 to 320 mas in 2000. At the same time, component B is fading and has almost disappeared in 2000 whereas the initially faint components C and D have become brighter. In 2001, the intensity level of component C has increased to almost 40% of the peak intensity of component A. Both components appear to have started merging in 2000.

These changes of the dust-shell appearance can be related to changes of the optical depths caused, e.g., by mass-loss variations. The present monitoring, covering more than 3 pulsational periods, shows that the structural variations are not related to the stellar pulsational cycle in a simple way. This is consistent with the predictions of hydrodynamical models that enhanced dust formation takes place on a timescale of several pulsational cycles (Fleischer et al. 1995).

Recent two-dimensional radiative transfer modelling (Men'shchikov et al. 2001) has shown that the star is surrounded by an optically thick dust shell with polar cavities of a full opening angle of 36°, which are inclined by 40° pointing with the southern lobe towards the observer. The bright and compact component A is not the direct light from the underlying central star but the southern lobe of this bipolar structure dominated by scattered light. Instead, the carbon star is at the position of the fainter northern component B.

5 The oxygen-rich AGB star CIT 3

CIT 3 is an oxygen-rich long-period variable star evolving along the AGB with extreme infrared properties. Due to substantial mass loss it is surrounded by an optically thick dust shell which absorbs almost all visible light radiated by the star and finally re-emits it in the infrared regime. The first near infrared bispectrum speckle-interferometry observations of CIT 3 in the J-, H-, and K'-band (resolution: 48 mas, 56 mas, and 73 mas) were obtained with the SAO 6 m telescope by Hofmann et al. (2001). While CIT 3 appears almost spherically symmetric in the H- and K'-band it is clearly elongated in the J-band along a symmetry axis of
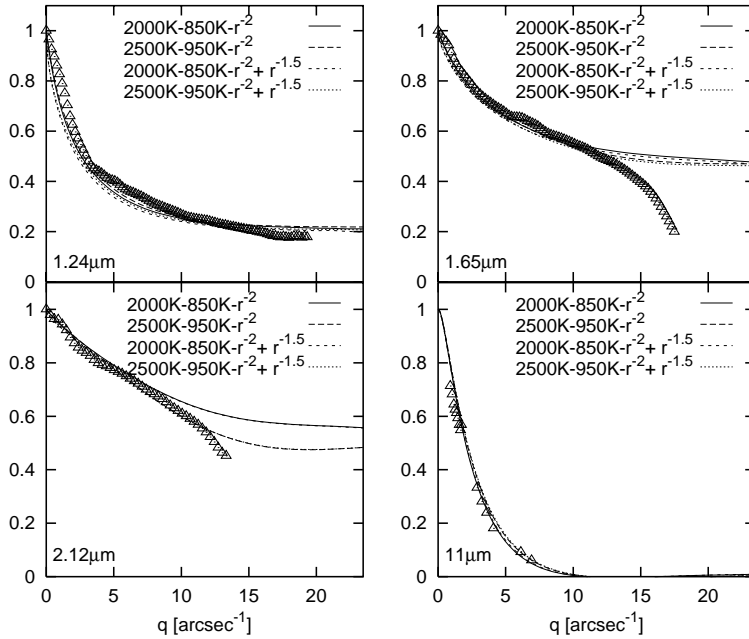
Fig. 4. CIT 3 model visibilities at $1.24\,\mu$m, $1.65\,\mu$m, $2.12\,\mu$m, and $11\,\mu$m for models with $(T_{\rm eff}, T_1)$=(2000 K,850 K) and (2500 K,950 K), resp. (Hofmann et al. 2001). Both uniform outflow models ($\rho \sim 1/r^2$; solid and long-dahed lines) and models with a flatter density distribution in the outer shell region ($\rho \sim 1/r^2$ for $Y \le 20.5$ and $\rho \sim 1/r^{1.5}$ for $Y > 20.5$; short-dashed and dotted lines) are shown. The optical depth $\tau_{0.55\mu{\rm m}}$ is 30. The symbols refer to the observations. Near-infrared visibilities — SAO 6m speckle observations. Mid-infrared visibility — ISI observations at 4m, 9.6m and 16m baseline of Lipman et al. (2000). For more details of the radiative transfer models and the fit of the spectral energy distribution, see Hofmann et al. (2001).

position angle $-28°$. Two structures can be identified: a compact elliptical core and a fainter north-western fan-like structure.

Extensive radiative transfer calculations have been carried out and confronted with the spectral energy distribution ranging from $1\,\mu$m to 1 mm, with the $1.24\,\mu$m, $1.65\,\mu$m and $2.12\,\mu$m visibility functions, as well as with 11μm ISI interferometry. The best model found to match the observations refers to a cool central star with $T_{\rm eff} = 2250$ K which is surrounded by an optically thick dust shell with $\tau(0.55\mu m) = 30$ (see Fig. 4). The central-star diameter is 10.9 mas and the inner dust shell diameter 71.9 mas. The inner dust-shell rim at $r_1 = 6.6R_*$ has a temperature of $T_1 = 900$ K. A two-component model consisting of an inner uniform-outflow shell region ($\rho \sim 1/r^2$, $r < 20.5r_1$) and an outer region where the density declines more shallow as $\rho \sim 1/r^{1.5}$ proved to give the best overall match of

the observations. Provided the outflow velocity stayed constant, the more shallow density distribution in the outer shell indicates that mass-loss has decreased with time in the past of CIT 3. Adopting $v_{exp} = 20$ km/s, the termination of that mass-loss decrease and the begin of the uniform-outflow phase took place 87 yr ago. The present-day mass-loss rate can be determined to be $\dot{M} = (1.3 - 2.1) \cdot 10^{-5}$ M$_\odot$/yr for $d = 500 - 800$ pc. A full description of these observations and models is given in Hofmann et al. (2001).

CIT 3 proved to be among the most interesting far-evolved AGB stars due to its infrared properties. Moreover, the aspherical appearance of its dust shell in the J-band puts it in one line with the few AGB stars known to expose near-infrared asphericities in their dust shells. The development of such asphericities close to the central star suggests that CIT 3 is in the very end of the AGB evolution or even in transition to the proto-planetary nebula phase where most objects are observed in axisymmetric geometry (Olofsson 1996). However, in contrast to other objects (as IRC+10216), CIT 3 shows these deviations from spherical symmetry only in the J-band, which is almost completely dominated by scattered light. This suggests that CIT 3 had just started to form aspherical structures and is in this regard still in the beginning of its final AGB phase. If so, CIT 3 is one of the earliest representatives of this dust-shell transformation phase known so far.

6   The rapidly evolving hypergiant IRC+10420

The star IRC+10 420 is an outstanding object for the study of stellar evolution since it is the only object currently being observed in its rapid transition from the red supergiant stage to the Wolf-Rayet phase. Its spectral type changed from F8 I$_a^+$ in 1973 (Humphreys et al. 1973) to mid-A today (Oudmaijer et al. 1996) corresponding to an increase of its effective temperature of 1000-2000 K within only 25 yr. It is heavily obscured by circumstellar dust due to strong mass loss with rates typically of the order of several 10^{-4} M$_\odot$/yr. IRC+10 420 can be classified as a luminous hypergiant with a mass of initially ~ 20 to 40 M$_\odot$.

Diffraction-limited 73 mas bispectrum speckle interferometry of IRC+10 420 (Blöcker et al. 1999) shows that the K-band visibility drops to 0.6 and then stays constant for frequencies > 4 cycles/arcsec revealing that the central star contributes $\sim 60\%$ and the dust shell $\sim 40\%$ to the total flux. To interpret these observations in more detail, radiative transfer calculations were conducted taking into account both SED and visibility. Again, single-shell models failed to reproduce the observations and a two-component shell was introduced assuming that IRC+10 420 had passed through a superwind phase in its history as can be expected from its evolutionary status. A previous superwind phase leads to changes in the density distribution, i.e. there is a region in the dusty shell which shows a density enhancement over the normal r^{-2} distribution. The best model for both SED and visibility was found for a dust shell with a dust temperature of 1000 K at its inner radius of $r_1 = 69 R_*$. At a distance of $308 R_*$ ($Y = r/r_1 = 4.5$), where the dust temperature has dropped to 480 K, the density was enhanced by a factor of $S = 40$ and its slope within the shell changed from $1/r^2$ to $1/r^{1.7}$. The angular

diameters of these components are 69 mas and 311 mas (stellar diameter $\sim$ 1 mas for $d = 5$ kpc). This can be interpreted in terms of a termination of an enhanced mass-loss phase roughly 90 years ago. The mass-loss rates of the components can be determined to be $\dot{M}_1 = 7.0 \ 10^{-5} \ M_{\odot}/\text{yr}$ and $\dot{M}_2 = 1.1 \ 10^{-3} \ M_{\odot}/\text{yr}$. We refer to Blöcker et al. (1999) for a full description of the model grid.

7   Simulating VLTI observations of IRC+10420

The above data (and model) of IRC+10420 rely on observations with the SAO 6 m telescope. Fig. 5 shows the visibility model predictions for different superwind amplitudes S up to a baseline of 110 m. Obviously, the various models can be best distinguished at longer baselines. Taking the corresponding model intensity distributions as input, Prygodda et al. (2001) presented computer simulations of interferometric imaging with VLTI/AMBER (ATs, wide-field mode) for IRC+10420. These simulations consider light propagation from the object to the detector as well as photon noise and detector read-out noise and show the dependence of the visibility error bar on various observational parameters. The results are shown in Fig. 5. Different seeing conditions for object and reference star turn out to be more crucial than, e.g., residual tip-tilt errors. With these simulations at hand one can immediately see under which conditions the visibility data quality would allow us to discriminate between the different model assumptions (here: the size of the superwind amplitude S). Inspection of Fig. 5 shows that in all studied cases the observations will give clear preference to one particular model. Therefore, observations with VLTI will certainly be well suited to prove theroretical predictions and to improve our current knowledge of this outstanding object.

8   Evolved Stars and the VLTI

VLTI observations with AMBER (see Petrov, this volume) and MIDI (see Perrin, this volume) will certainly have a large impact on the study of stars in late stages of stellar evolution revealing, for example, details of dust-shell structures and the mass-loss process. Radiative transfer calculations are an appropriate and efficient tool of interpreting these observations. However, for the robust and non-ambiguous construction of dust-shell models it is essential to take diverse and independent observational constraints into account. Apart from matching the spectral energy distribution, the consideration of spatially resolved information plays a crucial role for obtaining a reliable model. Generally speaking, as many pieces of spectral information as possible have to be taken into account. Visibilities at various wavelengths greatly constrain modelling, probing, for instance, scattering (J band) and thermal emission of hot dust (H, K band) and cool dust (N band). Near infrared visibilities can serve as sensitive indicators of the grain size. Furthermore, the combination of long-baseline interferometry data with high-resolution data at short baselines, as obtained, e.g., by bispectrum speckle interfermetry, will provide complementary information and will be of utmost value for modelling and interpretation (see, e.g., the case of IRC+10420).
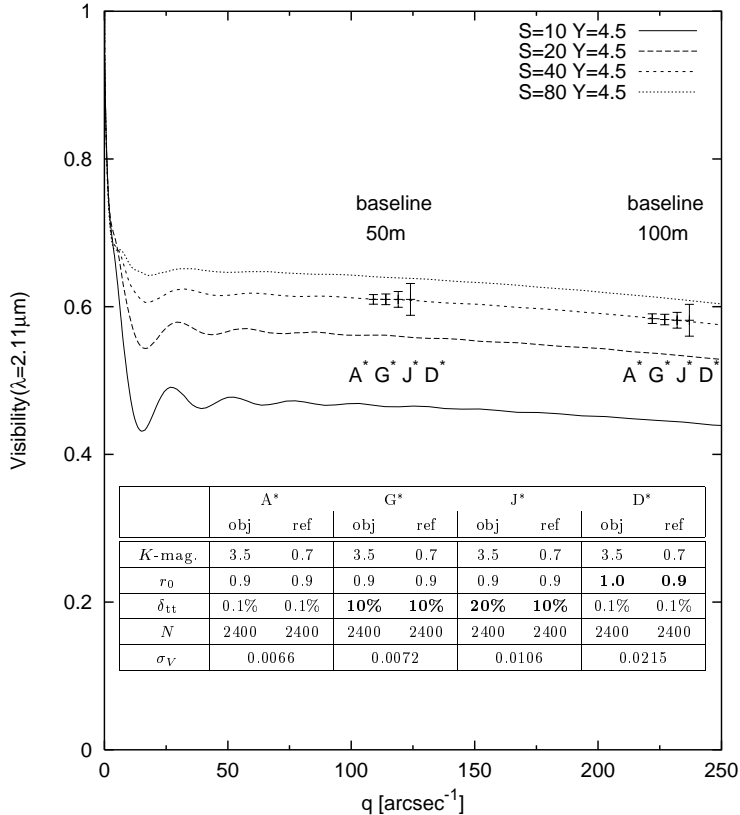
	A^* obj	A^* ref	G^* obj	G^* ref	J^* obj	J^* ref	D^* obj	D^* ref
K-mag.	3.5	0.7	3.5	0.7	3.5	0.7	3.5	0.7
r_0	0.9	0.9	0.9	0.9	0.9	0.9	**1.0**	**0.9**
δ_{tt}	0.1%	0.1%	**10%**	**10%**	**20%**	**10%**	0.1%	0.1%
N	2400	2400	2400	2400	2400	2400	2400	2400
σ_V	0.0066		0.0072		0.0106		0.0215	

Fig. 5. Dependence of the error bars of simulated AT-VLTI/AMBER (wide-field mode) observations of IRC +10 420 at 2.11 μm (Przygodda et al. 2001) on (i) seeing differences of object and reference star observations (Fried parameter, r_0, differences; simulation D^*), and (ii) different residual tip-tilt errors, δ_{tt}, of object and reference star observations (simulations G^* and J^*). Lines refer to radiative transfer models of different superwind amplitudes S. The symbols refer to AT-VLTI/AMBER simulations (each with N=2400 interferograms) of the S=40 intensity profile for baselines of 50 and 100 m (100 m: q=227 arc sec^{-1}). To better distinguish between the simulations, the data points belonging to one baseline are somewhat shifted with respect to the spatial frequency. The error bars are based on 6 statistically independent repetitions of each simulation.

For example, a near-infrared survey of dusty AGB stars with VLTI-AMBER should be based on a combination of various selection criteria comprising the existence of high-resolution single-dish observations, and/or prominent location in color-color (e.g. $J-K$ vs. K-[12]) and magnitude-color (e.g. K vs. K-[12]) diagrams indicative for the presence of dust, i.e. close vicinity to already resolved dusty objects. Dusty AGB objects resolved by speckle interferometry mostly show

$K-[12] \gtrsim 5$. Due to their thick dust shells, most of these stars are bright in K and observable with the VLTI without fringe tracking.

References

Blöcker T., Balega Y., Hofmann K.-H., Weigelt G., 2001, A&A 369, 142

Blöcker T., Balega Y., Hofmann K.-H., Lichtenthäler J., Osterbart R., Weigelt G., 1999, A&A 348, 805

Brandner W., Rousset G., Leuzen R., Hubin N., Lacombe F., Hofmann R., et al., 2002, Msngr 107, 1

Fleischer A.J., Gauger A., Sedlmayr E., 1995, A&A 297, 543

Haniff C.A., Buscher D.F., 1998, A&A 334, L5

Hofmann K.-H., Weigelt G., 1986, A&A 167, L15

Hofmann K.-H., Blöcker T., Balega Y., Weigelt G., 2001, A&A 379, 529

Humphreys R.M., Strecker D.W., Murdock T.L., Low, F.J., 1973, ApJ 179, L49

Ivezić Ž., Elitzur M., 1997, MNRAS 287, 799

Le Bertre T., 1992, A&AS 94, 377

Lipman E.A., Hale D.D., Monnier J.D., Tuthill P.G., Danchi W.C., Townes C.H., 2000, ApJ 532, 467

Lohmann A.W., Weigelt G., Wirnitzer B., 1983, Appl. Opt. 22, 4028

Loup C., Forveille T., Omont A., Paul J.F., 1993, A&AS 99, 291.

Men'shchikov A., Balega Y., Blöcker T., Osterbart R., & Weigelt G. 2001, A&A 368, 497

Olofsson H., 1996, ApSS 245, 169

Osterbart R., Balega Y., Blöcker T., Men'shchikov A., Weigelt G., 2000, A&A 357, 169

Oudmaijer R.D., Groenewegen M.A.T., Matthews H.E., Blommaert J.A.D.L, Sahu K.C., 1996, MNRAS 280, 1062

Przygodda F., Blöcker T., Hofmann K.-H., Weigelt G., 2001, Opt.Eng. 40, 753

Tuthill P.G., Monnier J.D., Danchi W.C., Lopez B., 2000, ApJ 543, 284

Tyson R.K., Bonaccini D., Roggemann M.C. (eds.), 2002, Adaptive Optics Systems and Technology II, Proc. SPIE Vol. 4494

Weigelt G., 1977, Optics Commun. 21, 55

Weigelt G., Balega, Y., Hofmann, K.-H., Langer, N., Osterbart, R., 1997, Science with the VLT Interferometer, ESO Astrophysics Symposia, p. 206

Weigelt G., Balega Y., Blöcker T., Fleischer A.J., Osterbart R., Winters J.M., 1998, A&A 333, L51

Weigelt G., Balega Y., Blöcker T., Hofmann K.-H., Men'shchikov A., Winters J.M., 2002, *Planetary Nebulae*, IAU Symp. 209, M. Dopita, S. Kwok, and R.S. Sutherland (eds.), Astronomical Society of the Pacific, in press

Winters J.M., Le Bertre T., Jeong K.S., Helling C., Selmayr E., 2000, A&A 361, 641